Electronic Supplementary Material (ESI) for Inorganic Chemistry Frontiers.

Supporting Information

Low-coordination single Ni atoms on graphitic C_3N_4 for nitrite electroreduction to ammonia

Hongyan Zhao [#], Jiaqi Xiang [#], Guike Zhang, Kai Chen, Ke Chu *

School of Materials Science and Engineering, Lanzhou Jiaotong University, Lanzhou 730070, China

[#] These authors contributed equally to this work.

*Corresponding author. chuk630@mail.lzjtu.cn (K. Chu)

Experimental Section

Synthesis of Ni_1/C_3N_4

Ni_1/C_3N_4 was synthesized by a thermal polymerization method. First, a mixture of 7 g of urea and 3 g of melamine was heated at 550 °C for 4 h to prepare the bulk g-C_3N_4, which was grinded to powder and subjected to 6 h of liquid exfoliation in anhydrous ethanol/deionized water (9:1 v/v) to obtain g-C_3N_4 nanosheets. Afterwards, 0.02 g of g-C_3N_4 was added to 30 mL of deionized water under sonication for 1 h, followed by adding 0.05 mL of 0.1 M $NiCl_2$ under stirring for 10 min. The mixed solution was standing for 1 h and then freeze-dried for 24 h to obtain Ni_1/C_3N_4.

Characterizations

X-ray diffraction (XRD) pattern was collected on a Rigaku D/max 2400 diffractometer. Transmission electron microscopy (TEM) and high-resolution transmission electron microscopy (HRTEM) were carried out on a Tecnai G^2 F20 microscope. Spherical aberration-corrected high-angle annular dark-field scanning transmission electron microscopy (AC HAADF-STEM) was performed on a Titan Themes Cubed G2 300 microscope.

Electrochemical experiments

Electrochemical measurements were carried out on a CHI-760E electrochemical workstation using a conventional three-electrode cell. The catalyst loaded on carbon cloth (CC, 0.5 mg/ cm^2) was used as the working electrode. Ag/AgCl and Pt foil were used as reference electrode and counter electrode, respectively. All potentials were referenced to reversible hydrogen electrode (RHE) by following equation: E_{RHE} (V)= $E_{Ag/Ag/Cl}$ + 0.198 + 0.059 × pH. The NO_2RR measurements were carried out in 0.5 M Na_2SO_4 containing 0.1 M $NaNO_2$ using an H-type cell separated by a Nafion 211 membrane. After each chronoamperometry test for 1 h, the produced NH_3 and other possible by-products were analyzed by various colorimetric methods using UV-vis absorbance spectrophotometer (MAPADA P5), while the gas products (H_2, N_2) were analyzed by gas chromatography (Shimadzu GC2010).

Determination of NH_3

NH_3 was quantitatively determined by the indophenol blue method[1]. Briefly, 2

mL NaOH solution (1 M) containing salicylic acid (5 wt%) and sodium citrate (5 wt%), 1 mL NaClO solution (0.05 M) and 0.2 mL Na[Fe(NO)(CN)$_5$] (1wt%) were respectively added into the 2 ml diluted electrolyte. After standing for 2 h, the UV-Vis absorption spectra was measured and the concentration-absorbance curves were calibrated by the standard NH_4Cl solution with a series of concentrations, and NH_3 yield rate and NH_3-Faradaic efficiency (FE_{NH3}) were calculated by the following equation:

NH_3 yield is calculated by

$$\mathrm{NH_3\ yield}\ (\mu \mathrm{g\ h^{-1}\ cm^{-2}}) = \frac{c_{\mathrm{NH_3}} \times V}{t \times A} \quad (1)$$

FE_{NH3} is calculated by

$$FE_{NH3}\ (\%) = \frac{6 \times F \times c_{\mathrm{NH_3}} \times V}{M \times Q} \times 100\% \quad (2)$$

where c_{NH3} (μg mL^{-1}) is the measured NH_3 concentration, V (mL) is the volume of the electrolyte, t (h) is the reduction time and A (cm^{-2}) is the area loading of the catalyst on CC, F (96500 C mol^{-1}) is the Faraday constant, M is the relative molecular mass of NH_3, Q (C) is the quantity of applied electricity.

Determination of N_2H_4

The concentration of N_2H_4 was determined by Watt and Chrisp method[2]. Typically, 5 mL of electrolyte was removed from the electrochemical reaction vessel. The 330 mL of color reagent containing 300 mL of ethyl alcohol, 5.99 g of $C_9H_{11}NO$ and 30 mL of HCl were prepared, and 5 mL of color reagent was added into the electrolyte. After stirring for 10 min, the UV-vis absorption spectrum was measured and the concentration-absorbance curves were calibrated by the standard N_2H_4 solution with a series of concentrations.

Calculation details

Spin-polarized DFT calculations were carried out using a Cambridge sequential total energy package (CASTEP). The Perdew–Burke–Ernzerhof (PBE) generalized gradient approximation (GGA) functional was used to model the exchange-correlation interactions. The DFT-D correction method was used to describe the van der Waals

interactions throughout the calculations. The electron wave functions were expanded using plane waves with a cutoff energy of 450 eV. The convergence tolerance was set to be 1.0×10^{-5} eV for energy and 0.03 eV $Å^{-1}$ for force. The Brillouin zone was sampled by 3×3×1 Monkhorst−Pack k-point mesh. The C_3N_4 was modeled by a 2×2 supercell, and a vacuum region of 15 Å was used to separate adjacent slabs. The adsorption energy (ΔE) is calculated as[3]

$$\Delta E = E_{ads/slab} - E_{ads} - E_{slab} \quad (3)$$

where $E_{ads/slab}$, E_{ads} and E_{slab} are the total energies for adsorbed species on slab, adsorbed species and isolated slab, respectively.

The computational hydrogen electrode (CHE) model was adopted to calculate the Gibbs free energy change (ΔG) for each elementary step as follows[3]

$$\Delta G=\Delta E + \Delta ZPE - T\Delta S \quad (4)$$

where ΔE is the adsorption energy, ΔZPE is the zero-point energy difference and $T\Delta S$ is the entropy difference between the gas phase and adsorbed state. The entropies of free gases were acquired from the NIST database.

Molecular dynamics (MD) simulations were carried out using a force field type of Universal. The electrolyte system was geometrically optimized by setting the convergence tolerance of 2.0×10^{-5} kcal/mol for energy and 0.001 kcal/mol/Å for force. The non-bond interaction was processed by Ewald with accuracy of 10^{-5} Kcal/mol and the repulsive cutoff was chosen as 12 Å. The electrolyte system was set up by randomly placing 50 H, 1000 H_2O and 50 NO_2^- in a simulation box. After geometry optimization, the MD simulations were performed under the universal field with the total simulation time of 5 ns at a time step of 1 fs.

The radial distribution function (RDF) is calculated as[4]

$$g(r) = \frac{dN}{4\pi\rho r^2 dr} \quad (5)$$

where dN is the amount of NO_2^-/H in the shell between the central particle r and $r+dr$, ρ is the number density of NO_2^-/H.

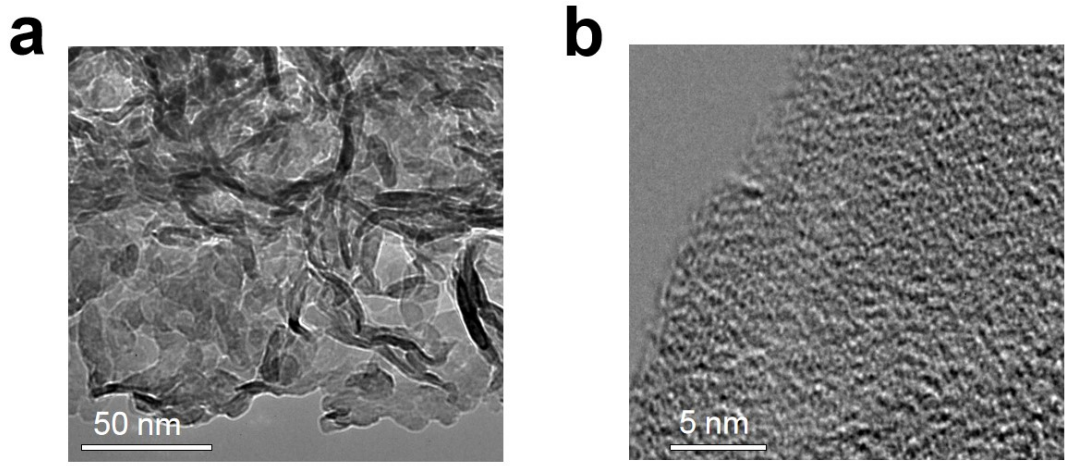

Figure S1. (a) TEM and (b) HRTEM images of pristine C_3N_4.

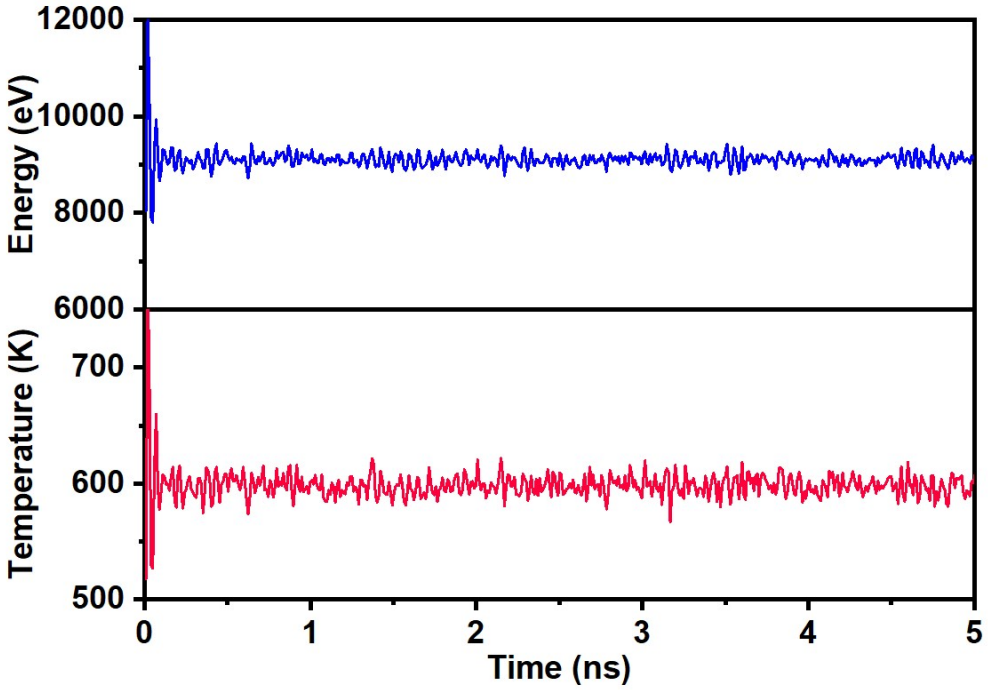

Figure S2. Variations of energy and temperature during the AIMD simulation for assessing the thermodynamic stability of Ni_1/C_3N_4.

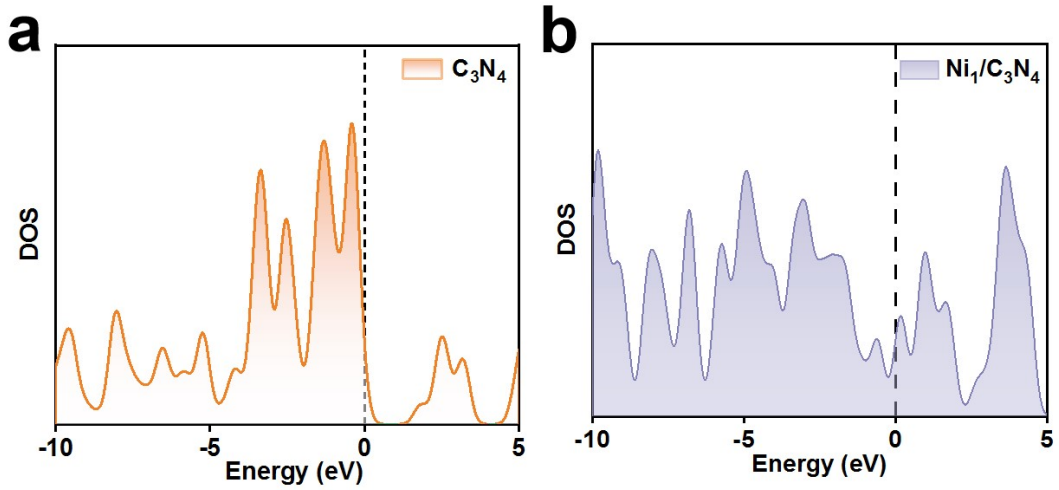

Figure S3. DOS profiles of (a) C_3N_4 and (b) Ni_1/C_3N_4.

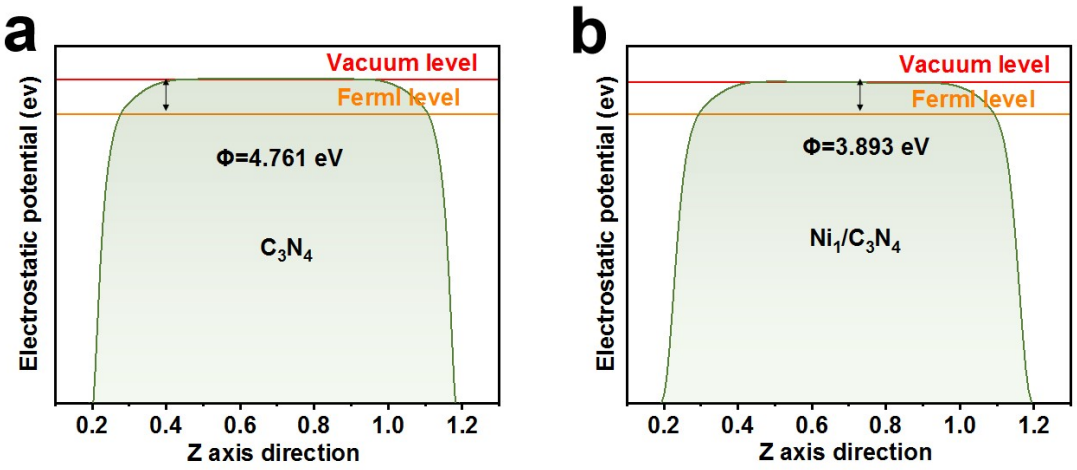

Figure S4. Average potential profiles along c-axis direction for calculating the work functions of (a) C_3N_4 and (b) Ni_1/C_3N_4.

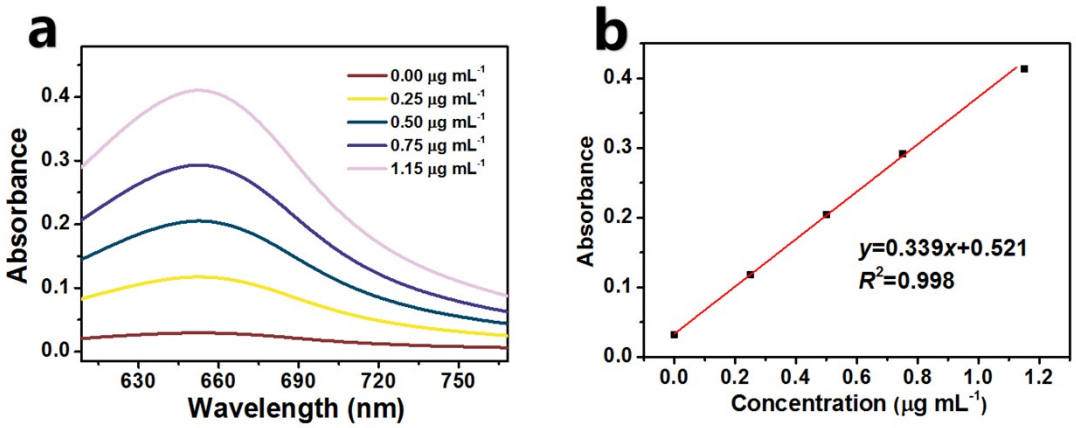

Figure S5. (a) UV-vis absorption spectra of NH_4^+ assays after incubated for 2 h at ambient conditions. (b) Calibration curve used for the calculation of NH_3 concentrations.

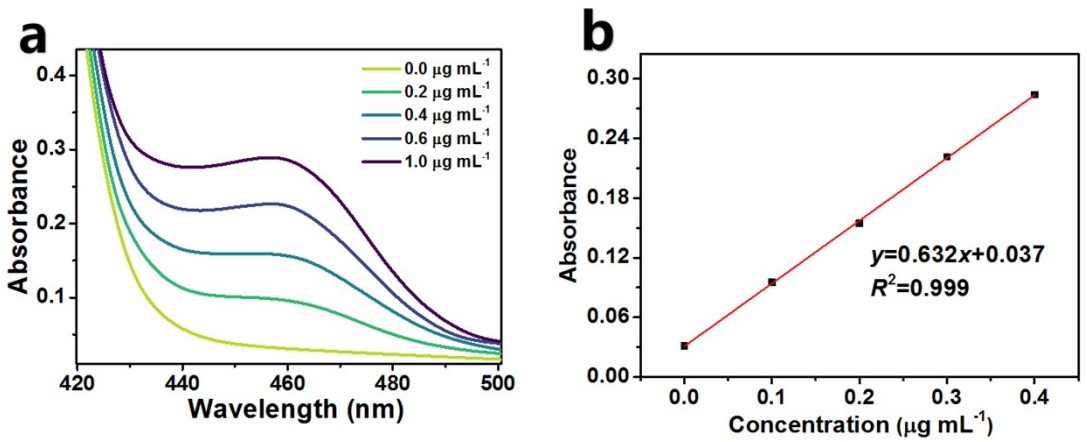

Figure S6. (a) UV-vis absorption spectra of N_2H_4 assays after incubated for 2 h at ambient conditions. (b) Calibration curve used for the calculation of N_2H_4 concentrations.

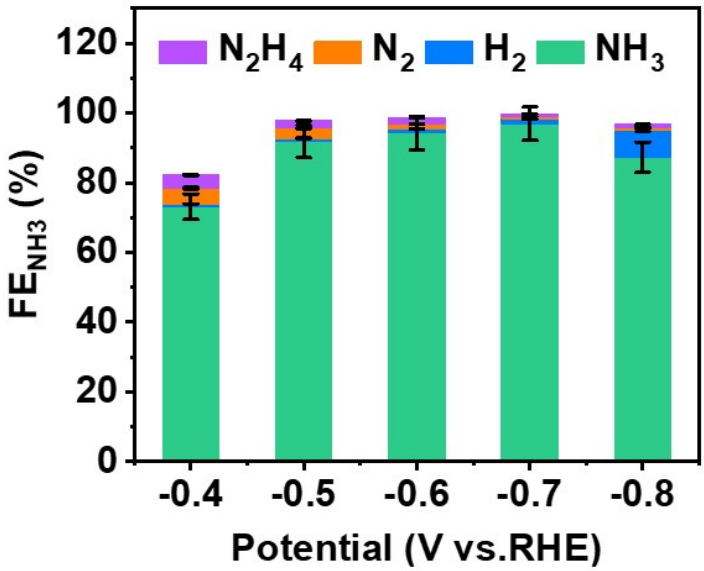

Figure S7. FEs of different products on Ni_1/C_3N_4 at various potentials.

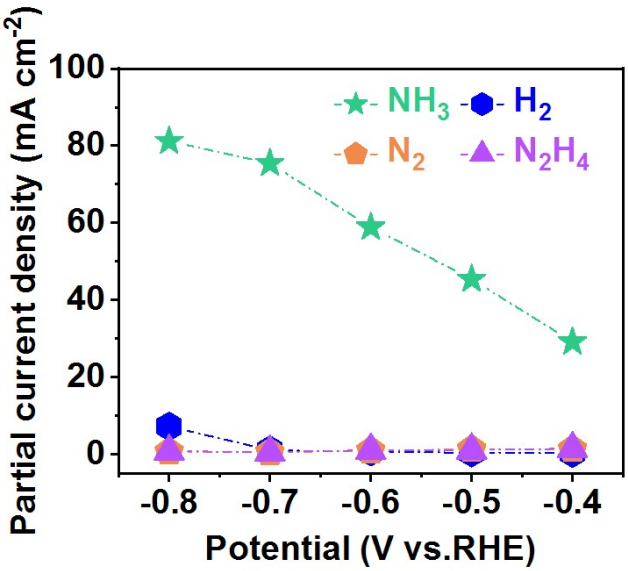

Figure S8. Partial current densities of various products on Ni_1/C_3N_4 at different potentials.

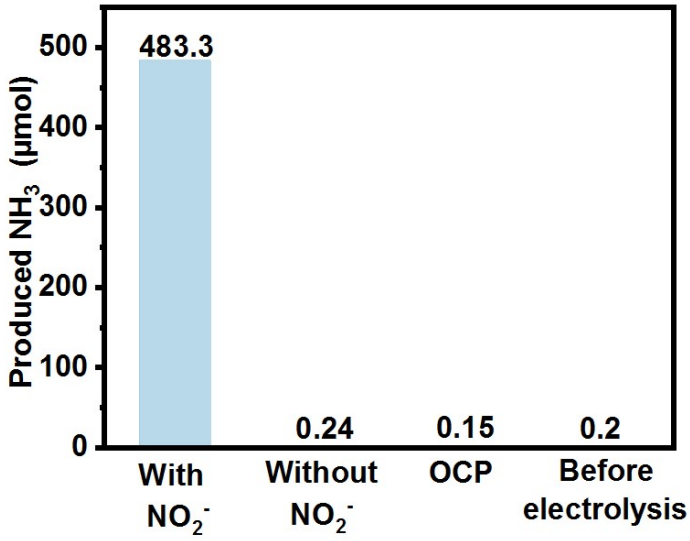

Figure S9. Amounts of produced NH_3 on Ni_1/C_3N_4 under different conditions: (1) electrolysis in NO_2^--containing solution at -0.7 V, (2) electrolysis in NO_2^--free solution at -0.7 V, (3) electrolysis in NO_2^--containing solution at open-circuit potential (OCP), (4) before electrolysis.

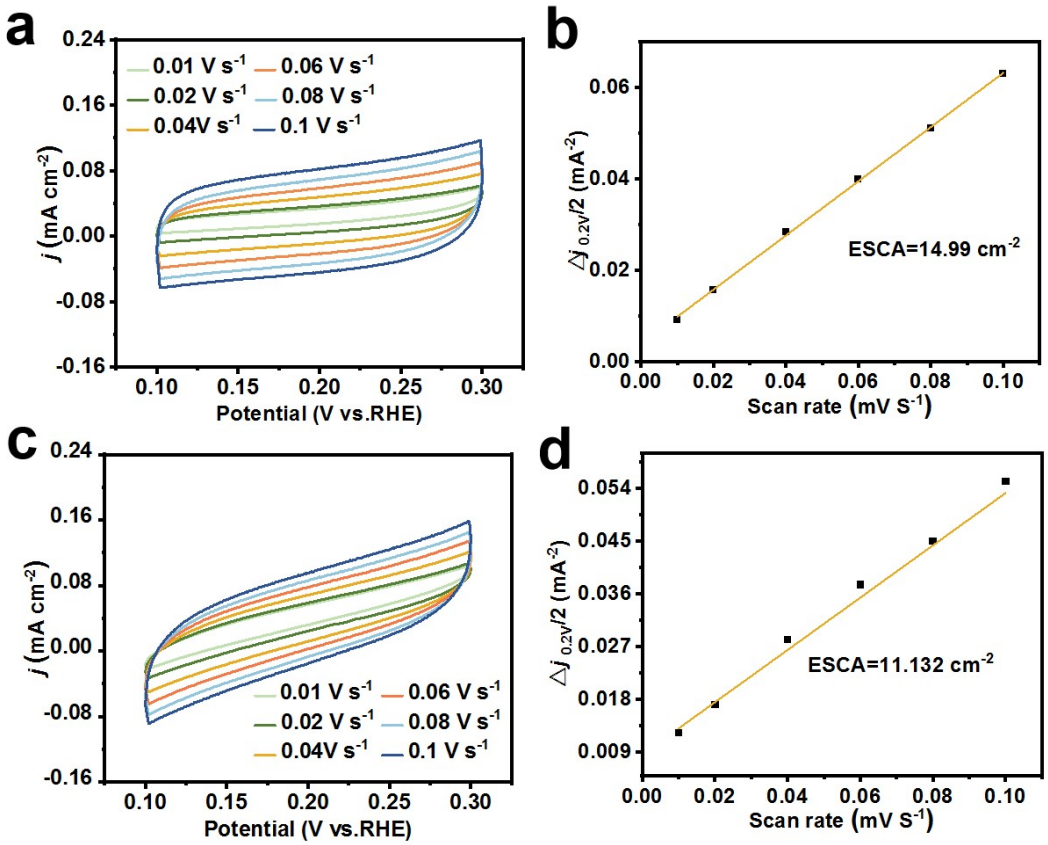

Figure S10. CV measurements at different scanning rates for (a, b) Ni_1/C_3N_4 and (c, d) C_3N_4, and corresponding calculated ECSA.

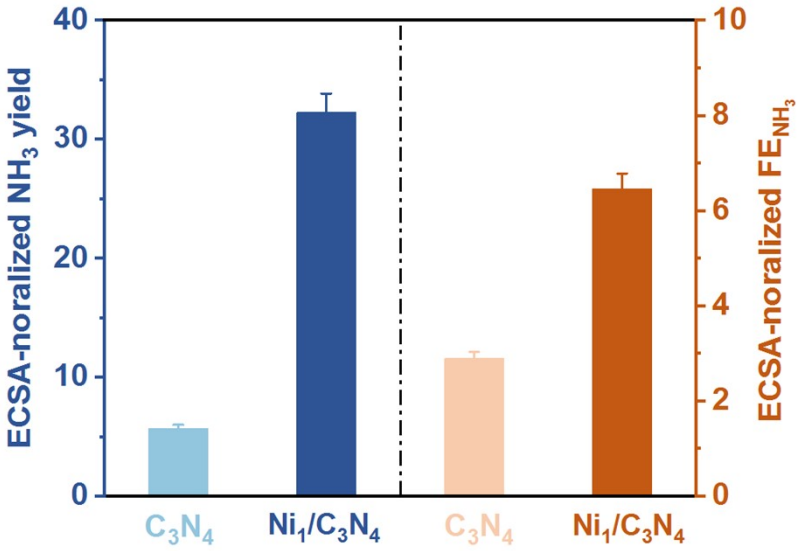

Figure S11. Comparison of the ECSA-normalized NH_3 yield rates and FE_{NH3} between C_3N_4 and Ni_1/C_3N_4 at -0.7 V.

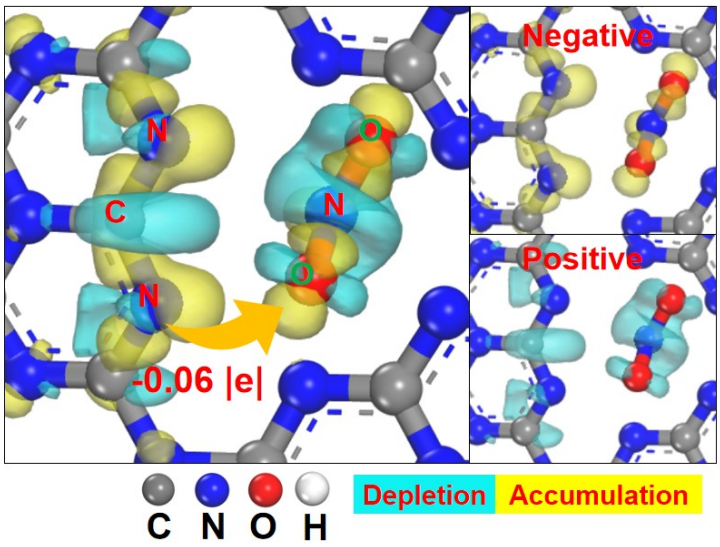

Figure S12. Charge density difference of absorbed NO_2^- on C_3N_4

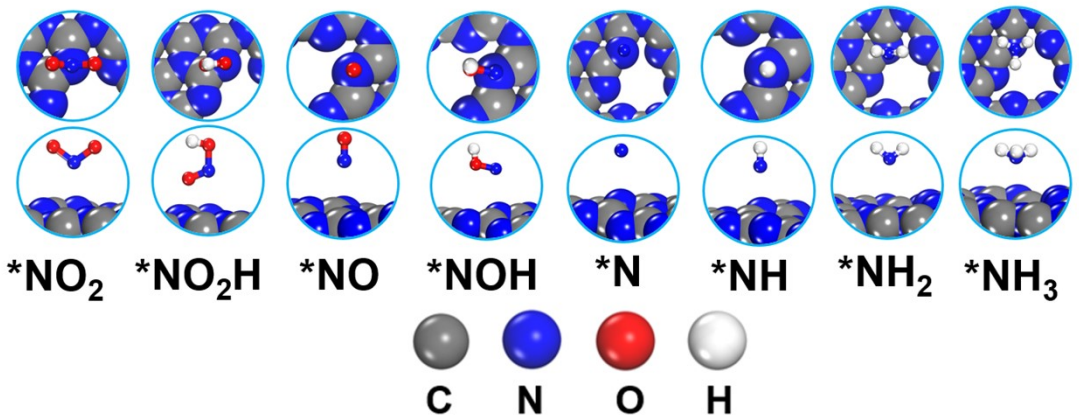

Figure S13. Optimized atomic structures of the reaction intermediates on C_3N_4.

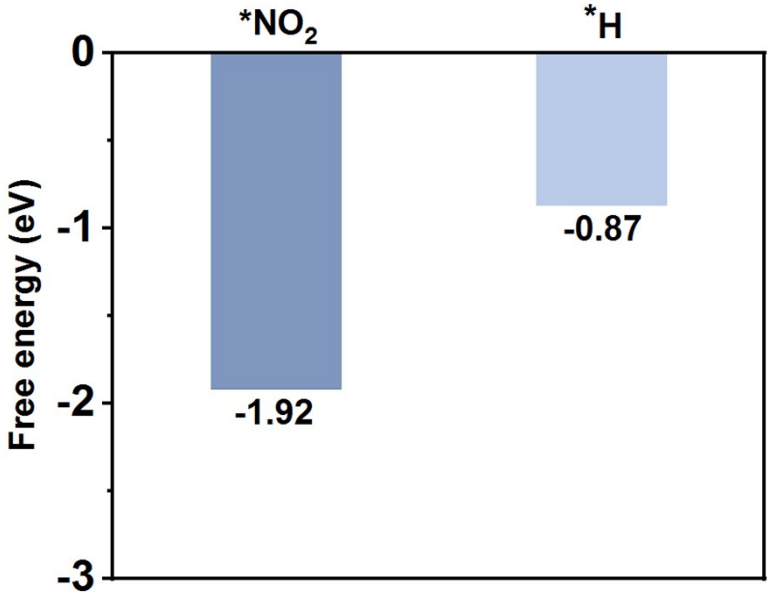

Figure S14. Binding free energies of *NO_2 and *H on Ni_1/C_3N_4.

Table S1. Structural parameters extracted from the EXAFS fitting results of Ni_1/C_3N_4

Sample	Shell	CN	R (Å)	σ^2 (10^{-3}Å)	ΔE_0 (eV)	R factor
Ni_1/C_3N_4	Ni-N	2.2	1.86	7.8	4.1	0.008

CN is the coordination number, R is interatomic distance, σ^2 is Debye-Waller factor, ΔE_0 is edge-energy shift, R factor is used to value the goodness of the fitting.

Table S2. Comparison of the optimum NH_3 yield and FE_{NH3} for the recently reported state-of-the-art NO2RR electrocatalysts at ambient conditions

Catalyst	Electrolyte	NH_3 yield rate ($\mu mol\ h^{-1}\ cm^{-2}$)	FE_{NH3} (%)	Potential (V vs RHE)	Ref.
$CoB@TiO_2/TP$	0.1 M Na_2SO_4 (0.1 M NO_2^-)	233.1	95.2	-0.7 V	5
Ag@NiO/CC	0.1 M NaOH (0.1 M NO_2^-)	235.4	97.7	-0.4 V	6
Cu/JDC/CP	0.1 M NaOH (0.1 M NO_2^-)	523.5	93.2	-0.6 V	7
$ITO@TiO_2/TP$	0.5 M $LiClO_4$ (0.1 M NO_2^-)	411.3	82.6	-0.5 V	8
$CF@Cu_2O$	0.1 M PBS (0.1 M NO_2^-)	441.8	94.2	-0.6 V	9
$Ni\text{-}TiO_2/TP$	0.1 M NaOH (0.1 M NO_2^-)	380.27	94.89	-0.5 V	10
$V\text{-}TiO_2/TP$	0.1 M NaOH (0.1 M NO_2^-)	540.8	93.2 @ -0.6	-0.7 V	11
$NiS_2@TiO_2/T$	0.1 M NaOH (0.1 M NO_2^-)	485.4	92.1	-0.5 V	12
Ni_2P/NF	0.1 M PBS (0.1 M NO_2^-)	191.3	90.2±3.0	-0.3 V	13
Ni_1/C_3N_4	**0.5 M Na_2SO_4 (0.1 M NO_2^-)**	**483.3**	**96.9**	**-0.7 V**	**This work**

Supplementary references

1. D. Zhu, L. Zhang, R. E. Ruther and R. Hamers, Photo-illuminated diamond as a solid-state source of solvated electrons in water for nitrogen reduction, *Nat. Mater.*, 2013, **12**, 836-841.
2. G. W. Watt and J. D. Chrisp, Spectrophotometric method for determination of hydrazine, *Anal. Chem.*, 1952, **24**, 2006-2008.
3. A. A. Peterson, F. Abild-Pedersen, F. Studt, J. Rossmeisl and J. K. Nørskov, How copper catalyzes the electroreduction of carbon dioxide into hydrocarbon fuels, *Energy Environ. Sci.*, 2010, **3**, 1311-1315.
4. K. Chu, Y. Luo, P. Shen, X. Li, Q. Li and Y. Guo, Unveiling the synergy of O-vacancy and heterostructure over MoO_{3-x}/MXene for N_2 electroreduction to NH_3, *Adv. Energy. Mater.*, 2022, **12**, 2103022.
5. L. Hu, D. Zhao, C. Liu, Y. Liang, D. Zheng, S. Sun, Q. Li, Q. Liu, Y. Luo, Y. Liao, L. Xie and X. Sun, Amorphous CoB nanoarray as a high-efficiency electrocatalyst for nitrite reduction to ammonia, *Inorg. Chem. Front.*, 2022, **9**, 6075-6079.
6. Q. Liu, G. Wen, D. Zhao, L. Xie, S. Sun, L. Zhang, Y. Luo, A. Ali Alshehri, M. S. Hamdy, Q. Kong and X. Sun, Nitrite reduction over Ag nanoarray electrocatalyst for ammonia synthesis, *J. Colloid Interf. Sci.*, 2022, **623**, 513-519.
7. L. Ouyang, L. Yue, Q. Liu, Q. Liu, Z. Li, S. Sun, Y. Luo, A. Ali Alshehri, M. S. Hamdy, Q. Kong and X. Sun, Cu nanoparticles decorated juncus-derived carbon for efficient electrocatalytic nitrite-to-ammonia conversion, *J. Colloid Interf. Sci.*, 2022, **624**, 394-399.
8. S. Li, J. Liang, P. Wei, Q. Liu, L. Xie, Y. Luo and X. Sun, ITO@TiO_2 nanoarray: An efficient and robust nitrite reduction reaction electrocatalyst toward NH_3 production under ambient conditions, *eScience*, 2022, **2**, 382-388.
9. Q. Chen, X. An, Q. Liu, X. Wu, L. Xie, J. Zhang, W. Yao, M. S. Hamdy, Q. Kong and X. Sun, Boosting electrochemical nitrite–ammonia conversion properties by a Cu foam@Cu_2O catalyst, *Chem. Commun.*, 2022, **58**, 517-520.
10. Z. Cai, C. Ma, D. Zhao, X. Fan, R. Li, L. Zhang, J. Li, X. He, Y. Luo, D. Zheng, Y. Wang, B. Ying, S. Sun, J. Xu, Q. Lu and X. Sun, Ni doping enabled improvement in electrocatalytic nitrite-to-ammonia conversion over TiO_2 nanoribbon, *Mater. Today Energy*, 2023, **31**, 101220.
11. H. Wang, F. Zhang, M. Jin, D. Zhao, X. Fan, Z. Li, Y. Luo, D. Zheng, T. Li, Y. Wang, B. Ying, S. Sun, Q. Liu, X. Liu and X. Sun, V-doped TiO_2 nanobelt array for high-efficiency electrocatalytic nitrite reduction to ammonia, *Mater. Today Phys.*, 2023, **30**, 100944.
12. X. He, L. Hu, L. Xie, Z. Li, J. Chen, X. Li, J. Li, L. Zhang, X. Fang, D. Zheng, S. Sun, J. Zhang, A. Ali Alshehri, Y. Luo, Q. Liu, Y. Wang and X. Sun, Ambient ammonia synthesis via nitrite electroreduction over NiS_2 nanoparticles-decorated TiO_2 nanoribbon array, *J. Colloid Interf. Sci.*, 2023, **634**, 86-92.
13. G. Wen, J. Liang, L. Zhang, T. Li, Q. Liu, X. An, X. Shi, Y. Liu, S. Gao, A. M. Asiri, Y. Luo, Q. Kong and X. Sun, Ni_2P nanosheet array for high-efficiency electrohydrogenation of nitrite to ammonia at ambient conditions, *J. Colloid Interf. Sci.*, 2022, **606**, 1055-1063.